HGG Advances

BRIEF COMMUNICATION

Epileptic encephalopathy linked to a *DALRD3* missense variant that impairs tRNA modification

Kejia Zhang,[1] Katharina Löhner,[2] Henny H. Lemmink,[2] Maartje Boon,[3] Jenna M. Lentini,[1] Naduni de Silva,[1] and Dragony Fu[1,4,*]

Summary

Epileptic encephalopathies are severe epilepsy syndromes characterized by early onset and progressive cerebral dysfunction. A nonsense variant in the DALR anticodon binding domain containing 3 (*DALRD3*) gene has been implicated in epileptic encephalopathy, but no other disease-associated variants in *DALRD3* have been described. In human cells, the DALRD3 protein forms a complex with the METTL2 methyltransferase to generate the 3-methylcytosine (m3C) modification in specific arginine tRNAs. Here, we identify an individual with a homozygous missense variant in *DALRD3* who displays developmental delay, cognitive deficiencies, and multifocal epilepsy. The missense variant substitutes an arginine residue to cysteine (R517C) within the DALR domain of the DALRD3 protein that is required for binding tRNAs. Cells derived from the individual homozygous for the DALRD3-R517C variant exhibit reduced levels of m3C modification in arginine tRNAs, indicating that the R517C variant impairs DALRD3 function. Notably, the DALRD3-R517C protein displays reduced association with METTL2 and loss of interaction with substrate tRNAs. Our results uncover another loss-of-function variant in *DALRD3* linked to epileptic encephalopathy disorders. Importantly, these findings underscore DALRD3-dependent tRNA modification as a key contributor to proper brain development and function.

Introduction

The post-transcriptional modification of tRNA has emerged as a critical modulator of biological processes ranging from gene expression to development.[1,2] In particular, tRNA modifications play critical roles in tRNA structure, stability, and function in protein synthesis.[3–5] Defects in tRNA modification have emerged as the cause of many types of human diseases, highlighting the critical role of tRNA modification in human health and physiology.[6–8] Notably, the brain appears to be sensitive to perturbations in tRNA modifications, as evidenced by the numerous neurological and neurodevelopmental disorders linked to deficiencies in tRNA modification.[9,10]

In mammalian cells, a subset of arginine tRNAs contain the 3-methylcytosine (m3C) modification at position 32 of the anticodon loop.[11,12] The m3C modification is hypothesized to stabilize the folding of the anticodon loop and has been shown to influence mitochondrial tRNA structure in human cells.[13,14] Thus, the m3C modification could affect the function of tRNAs in translation and protein expression (reviewed in Bohnsack et al.[15]). In human cells, the METTL2 methyltransferase forms a complex with the DALR anticodon binding domain containing 3 (DALRD3) protein to methylate tRNA-Arg-UCU and tRNA-Arg-CCU.[16] The DALRD3 protein recognizes specific arginine-tRNA isoacceptors to target them for methylation by the METTL2 methyltransferase. Human cells deficient in DALRD3 exhibit nearly complete loss of m3C in tRNA-Arg-UCU and Arg-CCU, demonstrating that DALRD3 plays a key role in m3C formation in specific arginine tRNAs.[16]

We have previously identified two sibling individuals with a homozygous nonsense variant in exon 9 of the *DALRD3* gene (rs1163930676, NM_001276405.1:c.1251C > A [p.(Tyr417*)]).[16] The C-to-A transversion introduces a premature stop codon in the *DALRD3* mRNA and results in the loss of DALRD3 protein expression. The two individuals were born from consanguineous parents who are heterozygous for the nonsense variant. The parents are healthy and do not exhibit any detectable pathologies. In contrast, the homozygous siblings display a collection of clinical symptoms classified as severe developmental and epileptic encephalopathy disorder.[17,18] Cells from the affected siblings exhibit a substantial reduction in m3C modification in tRNA-Arg-CCU and tRNA-Arg-UCU. These findings suggest a crucial biological role for DALRD3-dependent tRNA modification in development and nervous system function. However, the *DALRD3* nonsense allele represents the only case of a *DALRD3* variant that has been implicated in a neurodevelopmental disorder.

Here, we identify and characterize a *DALRD3* missense variant in an individual with developmental delay and epileptic encephalopathy. The person described here is characterized by a similar set of symptoms as the previously described individuals with nonsense variants in *DALRD3*. We demonstrate that fibroblast cells from the affected individual are greatly reduced in m3C modification in arginine tRNAs. Moreover, we demonstrate that

[1]Center for RNA Biology, Department of Biology, University of Rochester, Rochester, NY 14627, USA; [2]Department of Genetics, University of Groningen, University Medical Center Groningen, Groningen, the Netherlands; [3]Department of Neurology, University of Groningen, University Medical Center Groningen, Groningen, the Netherlands
[4]Lead contact
*Correspondence: dragonyfu@rochester.edu
https://doi.org/10.1016/j.xhgg.2024.100377.

Table 1. Clinical phenotype of individuals with homozygous variants in *DALRD3*

Individual	1 (this study)	2 (Lentini et al.[16])	3 (Lentini et al.[16])
ID	UMCG 2163660	19DG0509	19DG0510
Gender	male	male	female
Genotype	NM_001009996.2: c.1549C>T:	NM_001276405.1:c.1251C>A:	NM_001276405.1:c.1251C>A:
ClinVar	VCV002234459.2	VCV000918077.6	VCV000918077.6
ClinGen allele	CA2389547	CA352710392	CA352710392
GnomAD	3-49015671-G-A	3-49016236-G-T	3-49016236-G-T
Protein	p.(Arg517Cys)	p.(Tyr417*)	p.(Tyr417*)
Perinatal history	uncomplicated pregnancy, born term by cesarean section due to previous caesarean section	normal spontaneous vaginal delivery with history of placental insufficiency and oligohydramnios	Full-term product of caesarean section due to breech presentation, oligohydramnios, and placental insufficiency
Weight at birth (kg)	unknown	2.25 (−2.2 SD)	2.5 (fourth centile)
Developmental delay	severe[a]	severe	severe
Motor	progressively immobile,[b] can walk some steps unaided	immobile	immobile
Speech	speaks very few words[c]	nonverbal	nonverbal
Seizures	seizures started at age 4 years after febrile episode[d]; thereafter regression of psychomotor skills; focal clonic seizures with impaired awareness to bilateral seizures,[e,f] often in clusters up to 10, during the night/early morning; at age 15 years, interictal subtle myoclonus of the hands and fingers[g]	seizures started at age 7 months in the form of myoclonic jerks which remains frequent and poorly controlled by antiepileptic medications	at age 6 months epilepsy ensued, initially as brief episodes of flexion tonic spasm of head followed by myoclonic seizures; unlike the sibling brother, the epilepsy of affected individual 2 is reasonably controlled by antiepileptic medications
EEG	intermittent focal epileptic phenomena in temporal regions,[h] slow background activity without normal differentiation,[i] high-amplitude slow waves over frontotemporal regions	independent multifocal epileptic discharges predominantly over the anterior head region bilaterally as well as over the right temporal and right parietal regions	markedly high voltage and slow background for age along with slow generalized polyspike and wave activity
Tone	axial hypotonic,[j] extremities slightly hypertonic[k]; initially higher[l] and later low tendon reflexes[m] with extensor plantar responses; some ataxia of gait and hands[n,o]	axial and peripheral hypotonia with dystonic-like movement and generalized muscle wasting	central and peripheral hypotonia with dystonic-like movements and generalized muscle wasting
Microcephaly	no	no	yes
Brain finding	mild diffuse parenchymal volume loss[p]; normal aspect of white matter, basal ganglia, thalamus, and brain stem; arteriovenous malformation in right cerebellar hemisphere[q]; otherwise normal cerebellum; thickened skull by broad diploic space[r]	mild diffuse brain parenchymal volume loss with diffuse paucity of the myelin within the brain parenchyma	normal topographical and morphological appearance of the infratentorial and supratentorial structures
Audiology assessment	N/A	moderate to severe conductive hearing loss in left ear and mild conductive hearing loss in right ear	N/A
Dysmorphism	none; prepubertal at age 13 years[s]	subtle facial dysmorphia and small left ear	microcephaly with subtle facial dysmorphia

(*Continued on next page*)

Table 1. ***Continued***

Individual	1 (this study)	2 (Lentini et al.[16])	3 (Lentini et al.[16])
Other	marked lethargy and somnolence[t,u]; social interaction present, enjoys baby play; short stature (−3.7 SD) with delayed bone age[v]	severe gastroesophageal reflux disease necessitating gastronomy tube placement and fundoplication at age 4 years; no visual tracking or social smile	vomiting and choking on first day of life, mild congenital heart disease that resolved spontaneously, ectopic right kidney, bilateral optic disc pallor

[a]HP:0011344.
[b]HP:0002505.
[c]HP:0001344.
[d]HP:0002373.
[e]HP:0002266.
[f]HP:0002069.
[g]HP:0001336.
[h]HP:0010857.
[i]HP:0010845.
[j]HP:0008936.
[k]HP:0002509.
[l]HP:0001347.
[m]HP:0001315.
[n]HP:0002066.
[o]HP:0002070.
[p]HP:0002283.
[q]HP:0100026.
[r]HP:0000929.
[s]HP:0000823.
[t]HP:0001254.
[u]HP:0100786.
[v]HP:0004322.

the amino acid substitution caused by the missense variant abrogates the ability of DALRD3 protein to interact with substrate tRNAs. Our study reveals a loss-of-function variant in *DALRD3* linked to epileptic encephalopathy and further substantiates a role for DALRD3 protein function in ensuring proper neurodevelopment and neurological function.

Material and methods

Materials and methods can be found in the supplemental information.

Results

Based upon a match using the GeneMatcher platform,[19] we describe an individual exhibiting severe developmental delay and multi-focal epilepsy associated with a variant in *DALRD3* (Table 1, individual 1). The individual is a male of Sudanese ancestry who was born at term via cesarian section due to a previous cesarian section in the mother. Seizures started at age 4 years after a febrile episode followed by regression of psychomotor skills. The individual was referred to a pediatric neurologist again at 15 years of age for analysis because of progression of his symptoms. At neurological examination the affected individual displayed a dropped head and reduced facial expressivity (Figure 1A). In addition, he had progressive immobility, limited speech consisting of one-word expressions, increased muscle tone in his arms, subtle myoclonus, and ataxia. The individual has always had at least several epileptic seizures per month despite treatment with antiepileptic drugs at therapeutic doses (see the supplemental note in the supplemental information for the full clinical description).

Electroencephalogram (EEG) testing revealed slow background activity without normal differentiation, intermittent focal epileptic phenomena in temporal regions, and high-amplitude slow waves over frontotemporal regions (Figures 1B and S1). No microcephaly was detected, but MRI showed a relatively thin corpus callosum, widening of sulci and the ventricular system as a sign of parenchymal loss, and an arteriovenous malformation in the right cerebellar hemisphere (Figures 1C, 1D, and S2). Based upon the pattern and onset of symptoms, the individual matches clinical conditions classified as developmental and epileptic encephalopathy (DEE 86 [MIM: 618910]).[17]

We used exome sequencing of the affected individual followed by our previously described strategy of variant selection and classification to identify homozygous variants with potential pathogenicity (Table S1).[20] The candidate genes were then filtered by published association with epilepsy, which yielded a variant of unknown significance in the *DALRD3* gene (ClinVar: VCV002234459.2). The variant is a homozygous nucleotide substitution resulting in a C-to-T transition in the last exon of the *DALRD3* gene (rs140081609; MIM: 618904; Figures 2A and S3). Sanger sequencing confirmed the homozygous nucleotide substitution in the affected individual but not in a healthy control individual (Figure S4). The missense variant causes a substitution in the encoded DALRD3 protein of the canonical transcript (NM_001009996.3: c.1549C>T

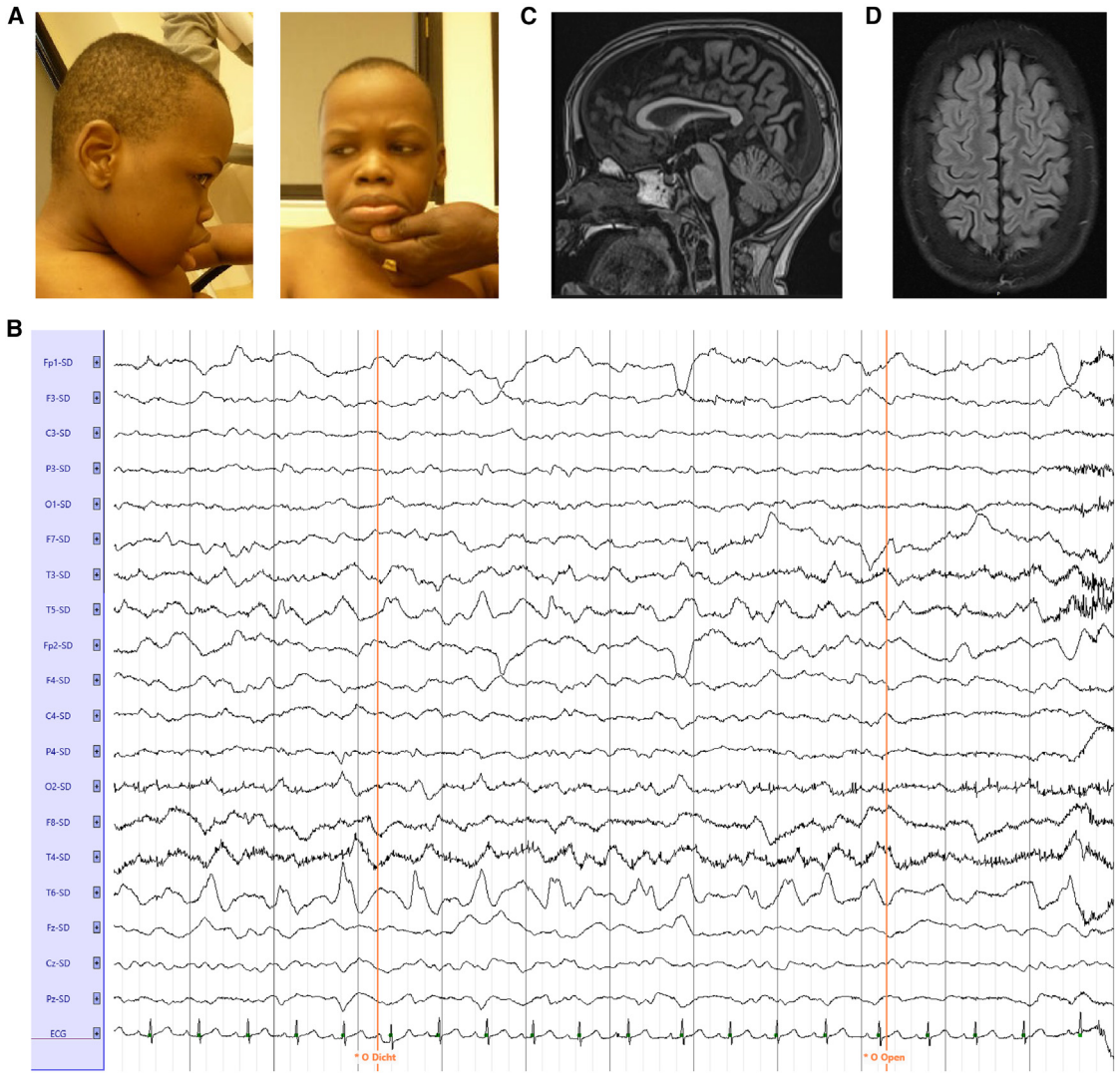

Figure 1. Identification of an individual exhibiting epileptic encephalopathy and brain pathologies
(A) Affected individual 2163660 containing a homozygous c.1549C>T (NM_001009996.3) variant in *DALRD3*.
(B) EEG trace; Laplacian montage with eyes closed and opened.
(C) MRI of the affected individual; sagittal T1 Magnetization Prepared Rapid Gradient Echo imaging.
(D) MRI of the affected individual; transversal T2 Turbo Spin Echo imaging.

[p.(Arg517Cys)]). Translation of this transcript is expected to produce a protein containing an arginine-to-cysteine substitution at position 517 (R517C) in the DALR tRNA anticodon-binding domain (Figure 2A, protein). The parents of the affected individual are consanguineous and heterozygous carriers of the *DALRD3* variant (Figures 2B and S5). Both parents are healthy with normal development and no detectable epilepsy. The *DALRD3* variant was not detected in the individual's older brother, who is healthy, developed normally, and did not exhibit epilepsy. The genotype of the sister is unknown, but she is healthy and exhibits normal development. These studies suggest that the R517C missense variant segregates with the disease in the family in an autosomal-recessive manner, being heterozygous in the parents, absent in the healthy sibling, and homozygous in the affected individual.

The *DALRD3* c.1549C>T (p.(Arg517Cys)) variant has been detected with an allele frequency of <0.00001 among 1,613,950 alleles screened, with 14 heterozygotes and 0 homozygotes identified thus far (gnomAD v.4.1.0, SNV: 3-49015671-G-A). The group frequency for this allele among individuals of African or African American ancestry is 0.00004 among 74,866 alleles tested. The genomic constraint of the surrounding 1 kb of sequence is 0.82, while the loss-of-function intolerant score for *DALRD3* is 0.

Sequence alignment reveals that the R517 residue of human DALRD3 protein is conserved in all known vertebrate DALRD3 orthologs from mammals to fish (Figure 2A). Based upon the high conservation in amino acid identity at this position, the nonsynonymous substitution caused by the R517C variant could disrupt the folding and function of the DARLD3 protein. Consistent with this hypothesis, the

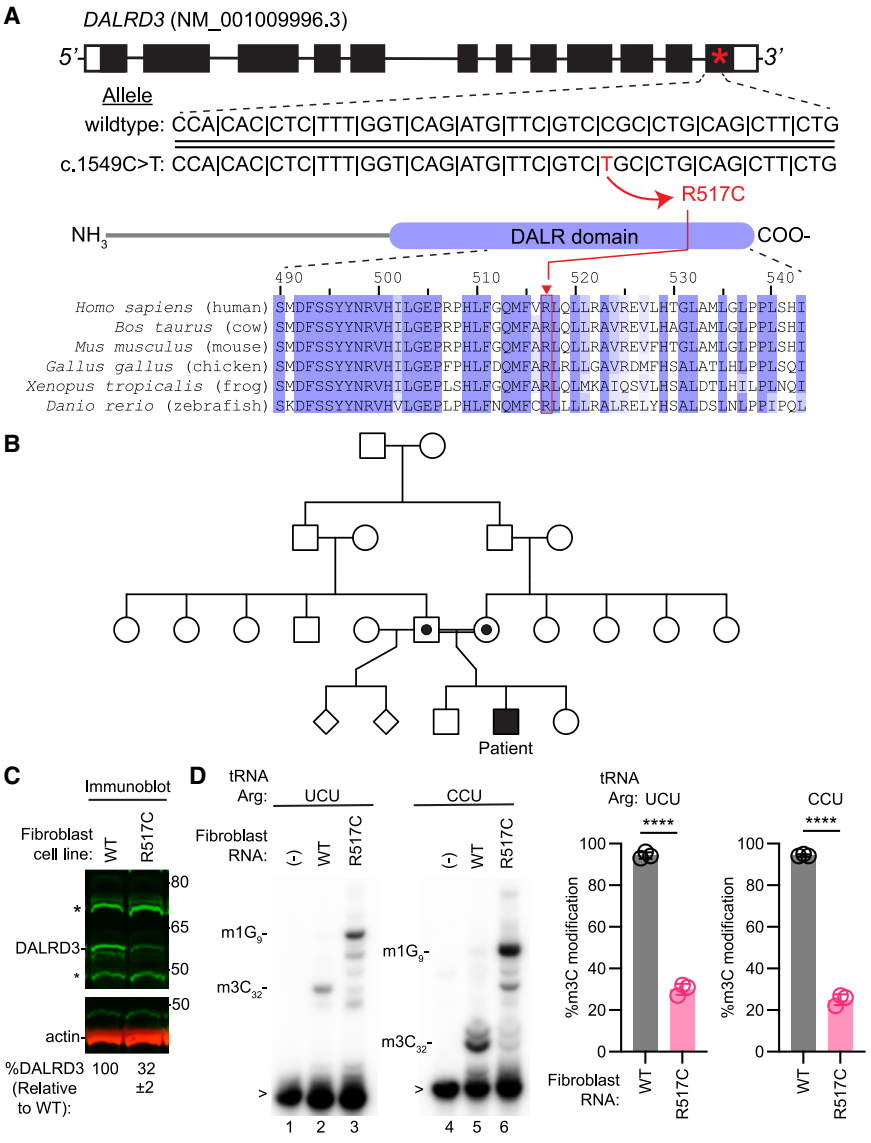

Figure 2. Identification of a missense variant in the *DALRD3* gene that impacts m3C modification status in arginine tRNAs

(A) *DALRD3* exon and intron structure with encoded protein shown below. An asterisk represents the location of the variant in the mRNA (NM_001009996.3). WT and c.1549C>T alleles are shown, with the variant shown in red. The schematic depicts the domain structure of the DALRD3 protein and alignment of the region encompassing the R517C variant.

(B) Pedigree of the family harboring the missense variant in the *DALRD3* gene.

(C) Immunoblot of lysates prepared from WT or R517 fibroblast cell lines. % DALRD3 represents the amount of DALRD3 protein relative to the WT fibroblast cell line and was quantified from three independent samples. ±, standard deviation from the mean.

(D) Primer extension analysis of tRNA-Arg-UCU and Arg-CCU extracted from WT or R517 fibroblast cell lines. (−) indicates that no RNA was added to the RT reaction. $m3C_{32}$, 3-methylcytosine. $m1G_9$, 1-methylguanine; >, labeled probe. Bar graphs represent quantification of m3C formation in tRNA-Arg-UCU or CCU by primer extension. $n = 3$. Error bars represent standard deviation from the mean. Significance was determined using an unpaired t test with two-tailed p value. ****$p \leq 0.0001$.

R517 variant is expected to be deleterious by multiple pathogenicity prediction algorithms (Figure S6).

To characterize the biological effects of the R517C variant on DALRD3 protein, we isolated fibroblast cells from the affected individual via skin biopsy (referred to as R517C fibroblast cells). We compared protein levels in the R517C fibroblast cells to fibroblast cells isolated from a healthy, age-matched control individual homozygous for the wild-type *DALRD3* alleles. Based upon immunoblotting, the levels of DALRD3 protein in the R517C fibroblast cells were greatly reduced compared to fibroblast cells from the healthy wild-type individual (Figure 2C). These results suggest that the R517C variant alters the structure of DALRD3, leading to reduced cellular stability and increased degradation.

We next tested the impact of the DALRD3-R517 variant on m3C modification in arginine tRNAs of fibroblast cells from the affected individual. We monitored m3C modification using a primer extension assay in which the presence of m3C leads to a reverse transcriptase (RT) block at position 32 of arginine tRNAs, while the lack of m3C allows for readthrough and generation of an extended product to the next RT block. Using this assay, we find that the m3C modification is greatly reduced in R517C fibroblast cells compared to control cells from a healthy individual (Figure 2D, quantified in bar graphs). These results demonstrate that R517C fibroblasts exhibit a deficiency in the m3C modification in specific tRNA-Arg isoacceptors. The deficit in m3C modification in the arginine tRNAs of R517C fibroblast cells provides evidence that the R517C variant causes partial loss of function.

These results indicate that the R517C variant in the DALRD3 protein impacts m3C modification in human cells. To elucidate the molecular defects associated with the R517C variant, we investigated the interaction between DALRD3 and METTL2. We co-transfected HEK293T cells with a plasmid expressing Streptactin (Strep)-tagged METTL2 along with empty vector or plasmids expressing a FLAG-tagged version of the wild type (WT) or the R517C DALRD3 variant (Figure 3A). Expression of METTL2, DALRD3-WT, or the DALRD3-R517C variant was confirmed by immunoblotting for the Strep tag or

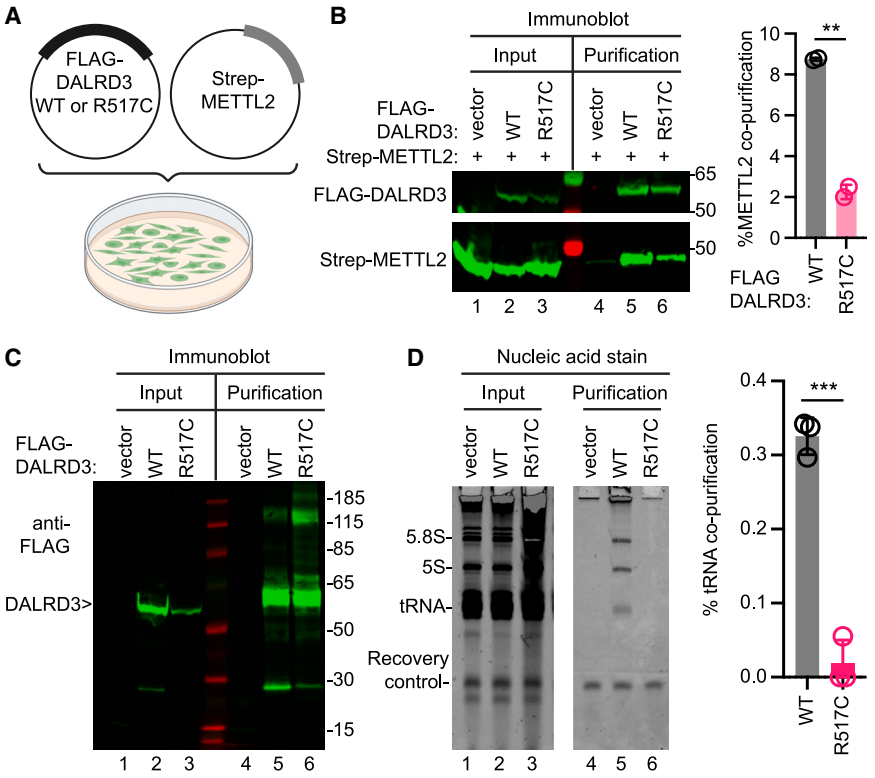

Figure 3. The DALRD3-R517C variant exhibits reduced co-precipitation with METTL2 and RNAs

(A) Co-transfection setup with plasmids encoding FLAG-DALRD3 and Strep-METTL2.

(B) Immunoblot of input lysates and anti-FLAG purifications from HEK293T cells transfected with the indicated plasmids. The immunoblot was probed with anti-FLAG and anti-Strep antibodies. Input represents 4% of the total sample used for purification. Purification represents 50% of the purified sample. Bar graph represents quantification of METTL2 co-purifying with DALRD3-WT or the R517C variant. The percentage of co-purifying METTL2 represents the amount of METTL2 in the purified DALRD3 sample that was recovered from the total input.

(C) Immunoblot of FLAG-DALRD3 purified from HEK293T cells. The immunoblot was probed with anti-FLAG antibodies. Input represents 4% of the total sample used for purification. Purification represents 20% of the total purified sample.

(D) Nucleic acid stain of RNAs extracted from the indicated input or purified samples after denaturing PAGE. The migration patterns of 5.8S rRNA (~150 nt), 5S rRNA (~120 nt), and tRNAs (~70–80 nt) are denoted. Input represents 2% of total extracts used for purification. The bar graph represents quantification of tRNA co-purifying with DALRD3-WT or the R517C variant. The percentage of tRNA co-purification represents the amount of tRNA in the purified DALRD3 sample that was recovered from the total input.

For bar graphs in (B) and (D), error bars represent standard deviation from the mean; significance was determined using an unpaired t test with two-tailed p value. **$p = 0.0015$ for (B). ***$p = 0.0002$ for (D).

FLAG tag (Figure 3B, input, lanes 1–3). We note that the DALRD3-R517C variant accumulated to lower levels than the WT DALRD3 protein in multiple independent transfections. The reduced levels of DALRD3-R517C protein compared to WT-DALRD3 in this system are consistent with the decreased amount of DALRD3 protein in the R517C fibroblast cells from the affected individual.

The FLAG-DALRD3 fusion proteins were then purified on anti-FLAG antibody resin, and recovery of FLAG-tagged DALRD3 was confirmed (Figure 3B, purification, FLAG-DALRD3, lanes 5 and 6). We detected an enrichment of METTL2 that copurified with DALRD3 above the background binding in the control purification (Figure 3B, purification, Strep-METTL2, compare lane 4 to lane 5). The amount of co-purifying METTL2 was decreased by ~4-fold with the DALRD3-R517C variant compared to DALRD3-WT after normalization to the amount of DALRD3 protein purified (Figure 3B, Strep-METTL2, compare lanes 5 and 6, quantified in the bar graph). This result suggests that the DALRD3-R517C variant exhibits less stable interaction with METTL2 compared to DALRD3-WT.

Based upon this finding, we next tested the interaction of DALRD3 with tRNAs. Like above, we transfected HEK293T cells with empty vector or plasmids expressing FLAG-DALRD3-WT or the DALRD3-R517C variant. Expression and purification of DALRD3-WT or the DALRD3-R517C variant was confirmed by immunoblotting for the FLAG tag (Figure 3C). We examined the RNA species that co-purified with DALRD3 by denaturing PAGE followed by nucleic acid staining. A recovery control RNA was included during RNA extraction to normalize for differences in recovery efficiency. While purification from vector-transfected cell lysates exhibited only background binding to tRNAs, the purified DALRD3-WT sample contained several co-purifying RNA species that correspond in size to tRNAs along with 5S and 5.8S rRNA (Figure 3D, compare lanes 4 and 5). This pattern of co-purifying RNAs is consistent with our previous observation that DALRD3 exhibits a stable interaction with rRNA and tRNAs that are targets for m3C modification.[16] In contrast to DALRD3-WT, the amount of co-purifying tRNAs with the DALRD3-R517C variant was reduced to nearly background levels (Figure 3D, quantified in the bar graph). Overall, these results reveal that the R517C substitution perturbs binding of DALRD3 to METTL2 and tRNAs.

Discussion

Altogether, we identify a loss-of-function variant in *DALRD3* that substantiates the link between DALRD3-dependent tRNA modification and neurological function.

Moreover, these results uncover the molecular basis for the deficit in tRNA modifications caused by the *DALRD3* missense variant. In particular, the decreased amount of DALRD3-R517C protein in the cell could contribute to a reduction in METTL2 and tRNA binding that impairs tRNA modification. Moreover, this result suggests that misfolding and loss of protein-RNA interactions promote degradation of the DALRD3-R517C protein by the ubiquitin-proteasome system. Interestingly, global analysis of the human ubiquitin-modified proteome has identified a ubiquitination site on lysine residue 28 of DALRD3 that is responsive to proteasome inhibition.[21] Thus, the levels of DALRD3 protein could potentially be restored in cells of affected individuals through proteasome inhibition.

The R517C substitution could also perturb the binding of METTL2 and tRNA substrates by affecting the folding of DALRD3 domains necessary for protein-RNA interactions. To gain insight into how the R517C substitution could affect DALRD3 folding, we mapped the R517 residue onto a predicted DALRD3 structure generated through AlphaFold.[22,23] DALRD3 is predicted to fold into an N-terminal region unique to DALRD3 homologs and a C-terminal DALR anticodon binding domain (Figure S7A, N-terminal region in gray, DALR domain in violet). The C-terminal DALR domain of DALRD3 is predicted to form an all α-helical bundle that is characteristic of DALR domains found in arginyl tRNA synthetases.[24,25] Based upon the AlphaFold model, the R517 residue lies within the last α helix of the all-α-helical bundle of the DALR domain, with the positively charged side chain partially exposed to solvent (Figures S7A and S7B, R517 residue in red). The change from an amphipathic arginine residue to a hydrophobic cysteine residue could alter the overall folding of the α-helical bundle of DALRD3 that impacts interactions with METTL2 and tRNAs. Moreover, the change from a positively charged arginine side chain to the uncharged cysteine side chain in DALRD3 could disrupt electrostatic or hydrogen bond interactions with METTL2 and arginine tRNAs.

The individual with the R517C variant in *DALRD3* exhibits many of the phenotypes displayed by two previously characterized individuals with a homozygous nonsense variant in *DALRD3*.[16] However, the onset of seizures in the individual described here was later in life compared to the two previously characterized individuals (4 years versus 6–7 months). Moreover, the individual described here exhibited less severe immobility and speech deficiencies compared to the two individuals with a homozygous nonsense variant. We also note that fibroblast cells from the individual with the R517C missense variant retain ~25% of the m3C modification in arginine tRNAs, while cells with the *DALRD3* frameshift variant exhibit nearly complete loss of m3C modification in arginine tRNAs.[16] Thus, the reduced severity of clinical symptoms associated with the R517C variant is consistent with the partial loss-of-function phenotype compared to the nearly complete loss of function in the *DALRD3* frameshift variant. Our findings set the stage for determining the biological pathways dependent upon DALRD3-dependent tRNA modifications that could be modulated in individuals with epileptic encephalopathy. Furthermore, our studies suggest that m3C modification status could serve as a functional assay to assist in the classification of uncharacterized *DALRD3* variants.

The different clinical presentations and ages of onset for individuals with *DALRD3* variants suggests that additional genes are likely to contribute to disease pathology. It is also possible that loss of DALRD3 protein function is independent of the observed phenotypes in families with *DALRD3* variants. Thus, the identification of additional individuals with *DALRD3* variants linked to disease will be the focus of future studies. Furthermore, the future generation of DALRD3-deficient animal models will provide a system for testing the role of DALRD3 function in neurodevelopment and brain function.

Data and code availability

The published article includes all data generated or analyzed during this study.

Acknowledgments

We thank the individuals and their family for participation in this study. We thank the Fu Lab for comments on this manuscript. This work was funded by NIH (USA) R01 GR532955 (to D.F.).

Declaration of interests

The authors declare no competing interests.

Web resources

ClinGen: https://clinicalgenome.org
ClinVar: https://www.ncbi.nlm.nih.gov/clinvar/
dbSNP: https://www.ncbi.nlm.nih.gov/snp/
gnomAD: https://gnomad.broadinstitute.org
gnomAD gene: https://gnomad.broadinstitute.org/gene/ENSG00000178149?dataset=gnomad_r4
gnomAD variant: https://gnomad.broadinstitute.org/variant/3-49015671-G-A?dataset=gnomad_r4
OMIM: https://www.omim.org

Supplemental information

Supplemental information can be found online at https://doi.org/10.1016/j.xhgg.2024.100377.

Received: July 18, 2024
Accepted: October 28, 2024

References

1. Zhang, W., Foo, M., Eren, A.M., and Pan, T. (2022). tRNA modification dynamics from individual organisms to metaepitranscriptomics of microbiomes. Mol. Cell. *82*, 891–906. https://doi.org/10.1016/j.molcel.2021.12.007.

2. Suzuki, T. (2021). The expanding world of tRNA modifications and their disease relevance. Nat. Rev. Mol. Cell Biol. *22*, 375–392. https://doi.org/10.1038/s41580-021-00342-0.
3. McCown, P.J., Ruszkowska, A., Kunkler, C.N., Breger, K., Hulewicz, J.P., Wang, M.C., Springer, N.A., and Brown, J.A. (2020). Naturally occurring modified ribonucleosides. Wiley Interdiscip. Rev. RNA *11*, e1595. https://doi.org/10.1002/wrna.1595.
4. Chujo, T., and Tomizawa, K. (2021). Human transfer RNA modopathies: diseases caused by aberrations in transfer RNA modifications. FEBS J. *288*, 7096–7122. https://doi.org/10.1111/febs.15736.
5. Smith, T.J., Giles, R.N., and Koutmou, K.S. (2024). Anticodon stem-loop tRNA modifications influence codon decoding and frame maintenance during translation. Semin. Cell Dev. Biol. *154*, 105–113. https://doi.org/10.1016/j.semcdb.2023.06.003.
6. Pereira, M., Francisco, S., Varanda, A.S., Santos, M., Santos, M.A.S., and Soares, A.R. (2018). Impact of tRNA Modifications and tRNA-Modifying Enzymes on Proteostasis and Human Disease. Int. J. Mol. Sci. *19*, 3738. https://doi.org/10.3390/ijms19123738.
7. Orellana, E.A., Siegal, E., and Gregory, R.I. (2022). tRNA dysregulation and disease. Nat. Rev. Genet. *23*, 651–664. https://doi.org/10.1038/s41576-022-00501-9.
8. Delaunay, S., Helm, M., and Frye, M. (2024). RNA modifications in physiology and disease: towards clinical applications. Nat. Rev. Genet. *25*, 104–122. https://doi.org/10.1038/s41576-023-00645-2.
9. Blaze, J., and Akbarian, S. (2022). The tRNA regulome in neurodevelopmental and neuropsychiatric disease. Mol. Psychiatr. *27*, 3204–3213. https://doi.org/10.1038/s41380-022-01585-9.
10. Ramos, J., and Fu, D. (2019). The emerging impact of tRNA modifications in the brain and nervous system. Biochim. Biophys. Acta. Gene Regul. Mech. *1862*, 412–428. https://doi.org/10.1016/j.bbagrm.2018.11.007.
11. Arimbasseri, A.G., Iben, J., Wei, F.Y., Rijal, K., Tomizawa, K., Hafner, M., and Maraia, R.J. (2016). Evolving specificity of tRNA 3-methyl-cytidine-32 (m3C32) modification: a subset of tRNAsSer requires N6-isopentenylation of A37. RNA *22*, 1400–1410. https://doi.org/10.1261/rna.056259.116.
12. Xu, L., Liu, X., Sheng, N., Oo, K.S., Liang, J., Chionh, Y.H., Xu, J., Ye, F., Gao, Y.G., Dedon, P.C., and Fu, X.Y. (2017). Three distinct 3-methylcytidine (m(3)C) methyltransferases modify tRNA and mRNA in mice and humans. J. Biol. Chem. *292*, 14695–14703. https://doi.org/10.1074/jbc.M117.798298.
13. Lentini, J.M., Bargabos, R., Chen, C., and Fu, D. (2022). Methyltransferase METTL8 is required for 3-methylcytosine modification in human mitochondrial tRNAs. J. Biol. Chem. *298*, 101788. https://doi.org/10.1016/j.jbc.2022.101788.
14. Kleiber, N., Lemus-Diaz, N., Stiller, C., Heinrichs, M., Mai, M.M.Q., Hackert, P., Richter-Dennerlein, R., Höbartner, C., Bohnsack, K.E., and Bohnsack, M.T. (2022). The RNA methyltransferase METTL8 installs m(3)C(32) in mitochondrial tRNAs(Thr/Ser(UCN)) to optimise tRNA structure and mitochondrial translation. Nat. Commun. *13*, 209. https://doi.org/10.1038/s41467-021-27905-1.
15. Bohnsack, K.E., Kleiber, N., Lemus-Diaz, N., and Bohnsack, M.T. (2022). Roles and dynamics of 3-methylcytidine in cellular RNAs. Trends Biochem. Sci. *47*, 596–608. https://doi.org/10.1016/j.tibs.2022.03.004.
16. Lentini, J.M., Alsaif, H.S., Faqeih, E., Alkuraya, F.S., and Fu, D. (2020). DALRD3 encodes a protein mutated in epileptic encephalopathy that targets arginine tRNAs for 3-methylcytosine modification. Nat. Commun. *11*, 2510. https://doi.org/10.1038/s41467-020-16321-6.
17. Scheffer, I.E., Berkovic, S., Capovilla, G., Connolly, M.B., French, J., Guilhoto, L., Hirsch, E., Jain, S., Mathern, G.W., Moshé, S.L., et al. (2017). ILAE classification of the epilepsies: Position paper of the ILAE Commission for Classification and Terminology. Epilepsia *58*, 512–521. https://doi.org/10.1111/epi.13709.
18. Scheffer, I.E., Zuberi, S., Mefford, H.C., Guerrini, R., and McTague, A. (2024). Developmental and epileptic encephalopathies. Nat. Rev. Dis. Prim. *10*, 61. https://doi.org/10.1038/s41572-024-00546-6.
19. Sobreira, N., Schiettecatte, F., Valle, D., and Hamosh, A. (2015). GeneMatcher: a matching tool for connecting investigators with an interest in the same gene. Hum. Mutat. *36*, 928–930. https://doi.org/10.1002/humu.22844.
20. Ghorbani, F., Alimohamed, M.Z., Vilacha, J.F., Van Dijk, K.K., De Boer-Bergsma, J., Fokkens, M.R., Lemmink, H., Sijmons, R.H., Sikkema-Raddatz, B., Groves, M.R., et al. (2022). Feasibility of Follow-Up Studies and Reclassification in Spinocerebellar Ataxia Gene Variants of Unknown Significance. Front. Genet. *13*, 782685. https://doi.org/10.3389/fgene.2022.782685.
21. Kim, W., Bennett, E.J., Huttlin, E.L., Guo, A., Li, J., Possemato, A., Sowa, M.E., Rad, R., Rush, J., Comb, M.J., et al. (2011). Systematic and quantitative assessment of the ubiquitin-modified proteome. Mol. Cell. *44*, 325–340. https://doi.org/10.1016/j.molcel.2011.08.025.
22. Jumper, J., Evans, R., Pritzel, A., Green, T., Figurnov, M., Ronneberger, O., Tunyasuvunakool, K., Bates, R., Žídek, A., Potapenko, A., et al. (2021). Highly accurate protein structure prediction with AlphaFold. Nature *596*, 583–589. https://doi.org/10.1038/s41586-021-03819-2.
23. Varadi, M., Anyango, S., Deshpande, M., Nair, S., Natassia, C., Yordanova, G., Yuan, D., Stroe, O., Wood, G., Laydon, A., et al. (2022). AlphaFold Protein Structure Database: massively expanding the structural coverage of protein-sequence space with high-accuracy models. Nucleic Acids Res. *50*, D439–D444. https://doi.org/10.1093/nar/gkab1061.
24. Wolf, Y.I., Aravind, L., Grishin, N.V., and Koonin, E.V. (1999). Evolution of aminoacyl-tRNA synthetases–analysis of unique domain architectures and phylogenetic trees reveals a complex history of horizontal gene transfer events. Genome Res. *9*, 689–710.
25. Delagoutte, B., Moras, D., and Cavarelli, J. (2000). tRNA aminoacylation by arginyl-tRNA synthetase: induced conformations during substrates binding. EMBO J. *19*, 5599–5610. https://doi.org/10.1093/emboj/19.21.5599.

HGGA, Volume *6*

Supplemental information

Epileptic encephalopathy linked to a *DALRD3* missense variant that impairs tRNA modification

Kejia Zhang, Katharina Löhner, Henny H. Lemmink, Maartje Boon, Jenna M. Lentini, Naduni de Silva, and Dragony Fu

Supplemental Information

Supplemental Note: Case Reports

The proband individual arrived in the Netherlands from Sudan via Egypt when he was almost 12 years old. Medical information on the individual's early childhood development is limited. The available information shows a history of normal pregnancy, delivery at term by uncomplicated caesarian section and normal neonatal period. Parents describe normal early development of the individual with the acquisition of language and walking. After a febrile episode at age 4 years, the individual started to have frequent epileptic seizures. There was a regression of his speech and motor functions.

EEG available from age six years during waking shows slowing of background activity in the left temporal area with superposition of spike and slow wave activity. An EEG at age eight years is described to be normal during waking. At that moment, the individual was being treated with valproic acid, at a serum level high within the therapeutic range. At age nine years, the EEG shows epileptic activity in the left temporal area with slow background activity, possibly also epileptic phenomena in the right temporal area. An EEG at age 13 years shows a diffuse encephalopathic pattern with multifocal epileptic phenomena, increasing during sleep with a temporal predominance on the right more than the left side, sometimes correlating with clinical phenomena.

The individual continues to have focal seizures with impaired awareness: tonic posturing of his right arm and rotation of the head and eyes towards the right side, shaking, crying, and sometimes vomiting with a duration of 30 seconds to one minute. The postictal phase lasts one to two minutes. He also has seizures lasting 5 seconds with a spasm of both arms and a scream. Sometimes the seizures generalize to bilateral clonic seizures. The seizures occur daily to weekly in clusters of one to seven seizures, a cluster lasting from one and a half hour to one and a half day. Despite treatment with various anti-epileptic drugs in therapeutic doses, the

individual has always had at least several epileptic seizures per month. Medication used was valproic acid, clobazam, lamotrigine, levetiracetam, also in combination.

Whole-exome sequencing

The raw sequencing data was processed using our in-house developed pipeline, as described previously[1]. The resulting Vcf files were uploaded into the Cartagenia/Alissa clinical informatics platform (version 5.1.4, Agilent Technologies). Variant selection, analysis and classification were performed as previously described[2]. First, quality filtering of the called variants was performed, excluding all those with a read depth 0.1% in the population databases were excluded from further analysis as they are considered benign. After filtering, variants were evaluated for their potential pathogenicity using in silico prediction software tools that are part of the Alamut Batch software (version 2.12; Interactive Biosoftware, Rouen, France), including SIFT, PolyPhen-2, MutationTaster, AlignGVGD, PhyloP and Grantham distance and four different splice site prediction programs (NNsplice, MaxEntScan, GeneSplicer and SpliceSiteFinder-Like). Variants were classified as “likely benign” (LB, class 2), “variant of uncertain significance” (VUS, class 3), “likely pathogenic” (LP, class 4) or “pathogenic” (P, class 5), largely based on ACMG guidelines[3]. In addition, we searched for scientific literature (PubMed and databases) that report identical or similar gene variants, including the Human Genome Mutation Database (HGMD) and ClinVar, for known (likely) pathogenic variants reported in patients.

Tissue culture

The DALRD3 R517C fibroblast cells were obtained by skin biopsy from the identified patient. The wildtype human fibroblast cell line was previously described and obtained from a healthy patient[4]. The 293T human embryonic cell line was obtained from ATCC (CRL-3216). Fibroblast and 293T cell lines were cultured in Dulbecco’s Minimal Essential Medium (DMEM)

supplemented with 10% fetal bovine serum (FBS), 1X penicillin and streptomycin (ThermoFisher), and 1X Glutamax (Gibco) at 37 °C with 5% CO2. Cells were passaged every 3 days with 0.25% Trypsin.

Western blotting of patient cell samples

Fibroblast cell lysates were prepared by resuspending cells in hypotonic lysis buffer (20 mM HEPES pH 7.9, 2 mM $MgCl_2$, 0.2 mM EGTA, 10% glycerol, 0.1 mM PMSF, 1 mM DTT) and incubation on ice for 5 minutes. The resuspended cells were subjected to three consecutive freeze-thaw cycles in liquid nitrogen and a 37 °C water bath. NaCl was added to the lysates to a final concentration of 0.4 M, incubated on ice for 5 minutes, and the lysates spun at 14,000 × g for 15 min at 4 °C. After centrifugation, the supernatant was collected, and flash frozen in liquid nitrogen before storage at -80 °C.

Cellular extracts and purified protein samples were fractionated on NuPAGE Bis-Tris polyacrylamide gels (Thermo Scientific) followed by transfer to Immobilon FL PVDF membrane (Millipore) for immunoblotting. Antibodies were against the following proteins : DALRD3 (MA1-21315, Thermo Fisher), FLAG (NC9261069, Thermo Fisher), and actin (CST). Primary antibodies were detected using IRDye 800CW Goat anti-Mouse IgG (SA5-35521, Thermo Fisher) or Rabbit (SA5-35571, Thermo Fisher) or IRDye 680RD Goat anti-Mouse IgG (926-68070, LI-COR Biosciences) or goat anti-Rabbit IgG (925-68071). Immunoblots were scanned and quantified using direct infrared fluorescence via the Odyssey System and Image Studio software (LI-COR Biosciences).

Primer extension analysis

Total RNA from human cells was extracted and purified using TRIzol LS reagent (Thermo Fisher). Primer extension was performed as previously described[5]. Briefly, 3 µg of total RNA was pre-annealed with a 5′-^{32}P-radiolabelled oligonucleotide complementary to tRNA-Arg-

UCU or CCU. The mixture was heated at 95 °C for 3 minutes followed by slow cooling to 45 °C. After cooling, 14 µl of extension mix (0.12 µl of avian myeloblastosis virus reverse transcriptase (Promega), 2.8 µl 5X RT buffer, 1.12 µl 1 mM dNTPs, RNase-free water to 14 µl) was added to each reaction and incubated at 45 °C for 1 hour. Samples were mixed with 2x formamide denaturing dye, heated to 95 °C for 3 minutes and resolved on an 20% polyacrylamide, 7 M urea, 1xTBE denaturing gel. Phosphorimaging was performed on an Azure Sapphire phosphorimager and analyzed using NIH ImageJ software.

Transient transfections and protein-RNA purifications.

293T cells were transfected via calcium phosphate transfection method. Briefly, 2×10^6 cells were seeded on 100 × 20 mm tissue culture grade plates (Corning) followed by transfection with 20 µg of plasmid DNA. After 48 hours post-transfection, cells were dissociated from the plate using trypsin, harvested at 700 × g for 5 minutes followed by washing with PBS. Cell pellets were resuspended in 0.5 mL of hypotonic lysis buffer (20 mM HEPES pH 7.9, 2 mM MgCl2, 0.2 mM EGTA, 10% glycerol, 0.1 mM PMSF, 1 mM DTT). Cells were kept on ice for 5 minutes followed by three freeze-thaw cycles in liquid nitrogen and a 37 °C water bath. NaCl was added to the lysates to a final concentration of 0.4 M, incubated on ice for 5 minutes and the lysates spun at 14,000 × g for 15 min at 4 °C. After centrifugation, 500 µl of the lysate was removed and diluted with an equal volume of hypotonic lysis buffer containing 0.2% NP-40. Cell lysates were flash frozen in liquid nitrogen and stored at -80 °C.

FLAG-tagged proteins were purified by incubating whole cell lysates with 50 µl of MonoRab Anti-DYKDDDDK Magnetic Beads (GenScript) for two hours at 4 °C. Magnetic resin was washed three times with 1X HLB200 (20 mM HEPES pH 7.9, 2 mM $MgCl_2$, 0.2 mM EGTA, 10% glycerol, 0.1% NP-40, 200 mM NaCl, 0.1 mM PMSF, 1 mM DTT). Proteins were eluted by resuspending resin in 1X NuPAGE LDS Sample Buffer supplemented with 50 mM DTT and heating at 95 °C for 5 minutes. Input lysates and purified proteins were fractionated on a

NuPAGE Bis-Tris PAGE (ThermoFisher) and transferred to Immobilon-FL PVDF Membrane (Millipore Sigma). Immunoblotting was performed as described above. The percent METTL2 co-purification was determined by dividing the METTL2 signal in the DALRD3 purification by the total amount of METTL2 in the starting extract after normalization to the total amount of DALRD3 purified.

For RNA copurification analysis, the resin was resuspended in 100 µL of Molecular Biology Grade RNAse-free water (Corning). 15 µl of the resuspended resin was taken for immunoblotting analysis where the beads were mixed with 5 µl of 4X NuPAGE LDS Sample Buffer supplemented with 50 mM DTT and heating at 95 °C for 5 minutes prior to loading onto a NuPAGE Bis-Tris PAGE (ThermoFisher). RNA extraction followed the TRIzol LS RNA extraction protocol (Invitrogen). Recovery control RNA (20 ng) was added to the purified bead samples. RNA was resuspended in 10 µl of RNAse-free water and loaded onto a 10% polyacrylamide, 7 M urea gel. The gel was then stained with SYBR Gold nucleic acid stain (Invitrogen) to visualize RNA. The amount of RNA co-purified with DALRD3 was determined by dividing the tRNA signal in the DALRD3 purification by the total amount of tRNA signal in the starting extract after normalization to the total amount of DALRD3 purified.

Ethics approval and consent to participate

IRB of University Medical Centre of Groningen gave ethical approval for this work. The patient and family provided consent for participation in the study and publication of the results.

Availability of data and materials

All data and materials are available upon request.

Supplemental Figure 1. Epileptiform discharges detected at the right temporal electrode during EEG testing of the patient in this study. (A) Bipolar and (B) Laplacian montages.

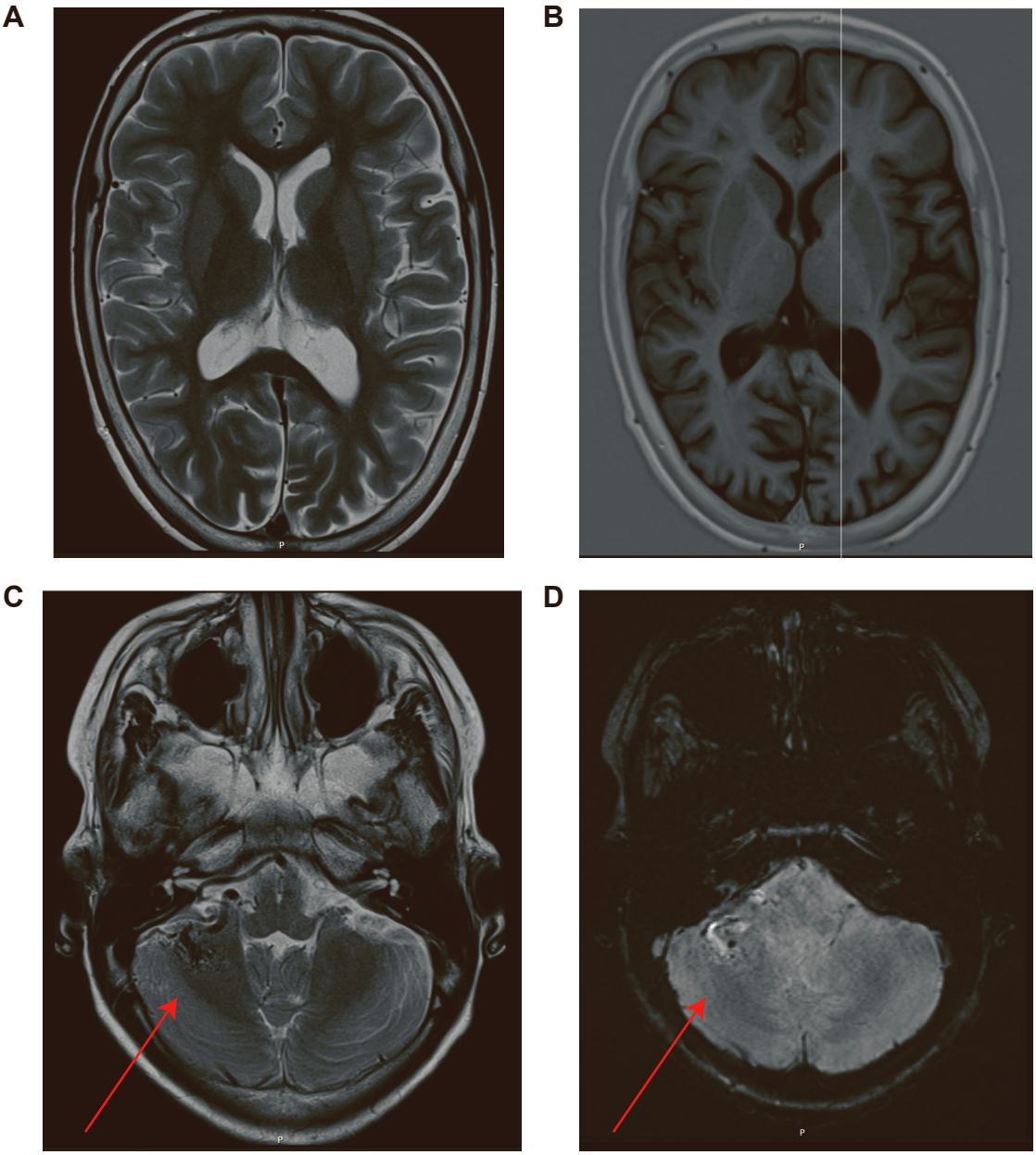

Supplemental Figure 2. The individual in this study exhibits enlargement of sulci and ventricular system along with a right cerebellar arteriovenous malformation. (A) MRI at 13 years of age; transversal T2 TSE. (B) MRI; transversal T1 TSE (C) Transversal T2 TSE weighted MRI scan. (D) Transversal SWI (susceptibility weighted) scan. Arrow points at the right cerebellar arteriovenous malformation.

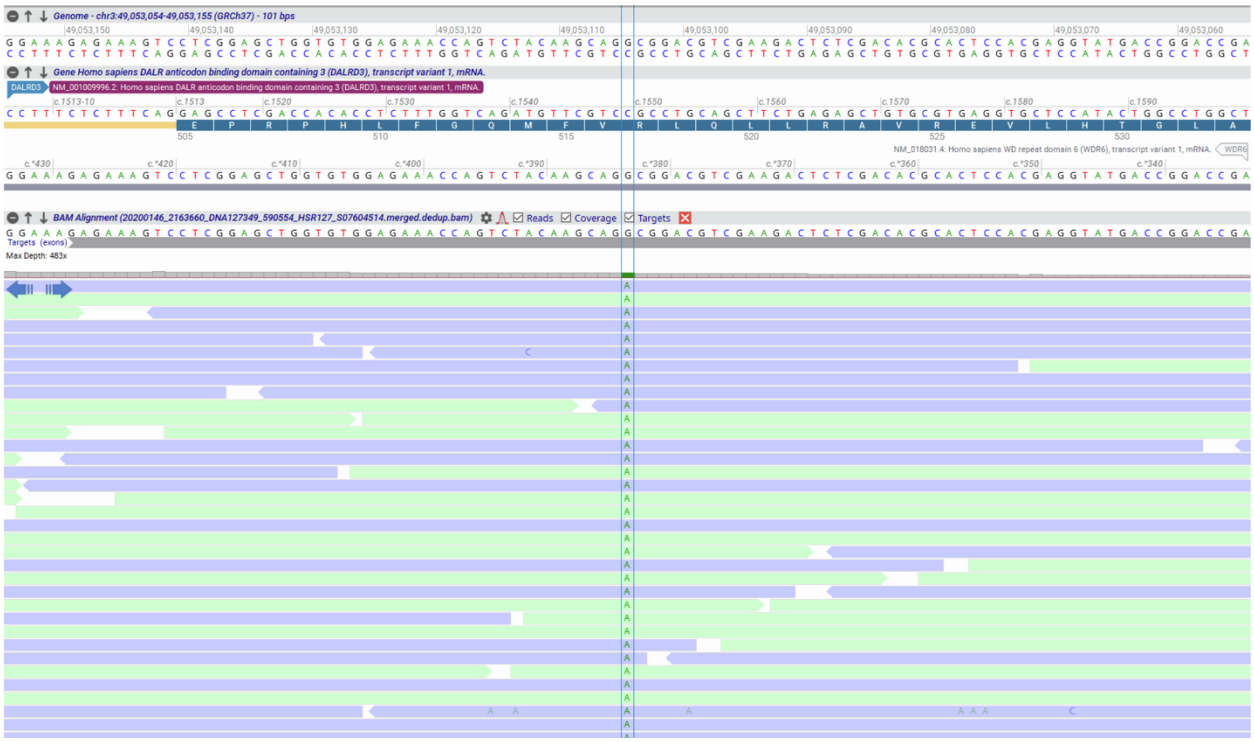

Supplemental Figure 3. Identification of a homozygous missense variant in the *DALRD3* gene of the patient in this study. Whole exome sequence analysis output.

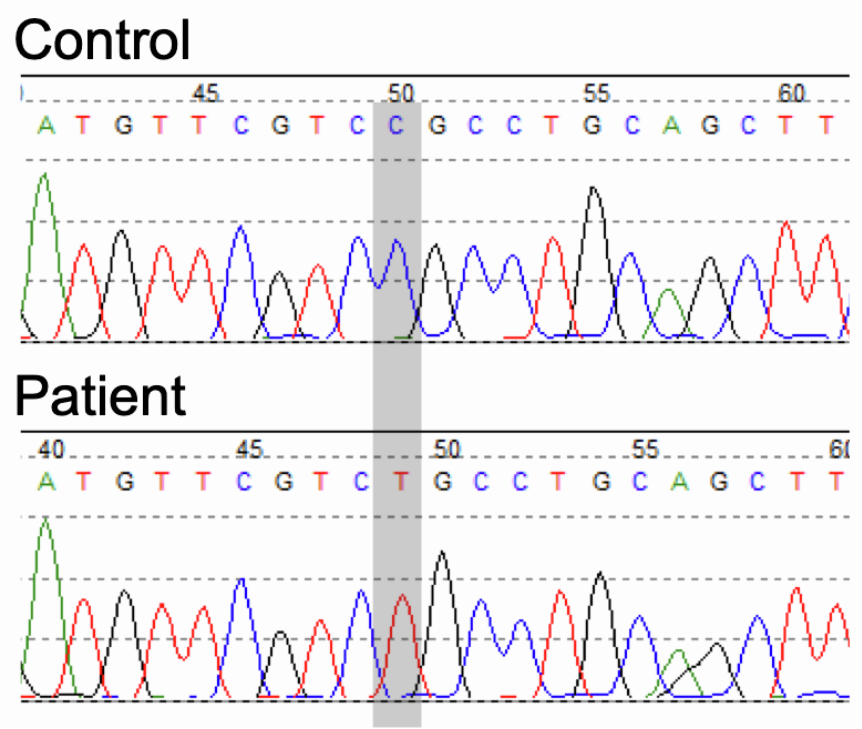

Supplemental Figure 4. Sanger sequencing chromatograms of a healthy, control individual and the patient characterized in this study.

A Mother

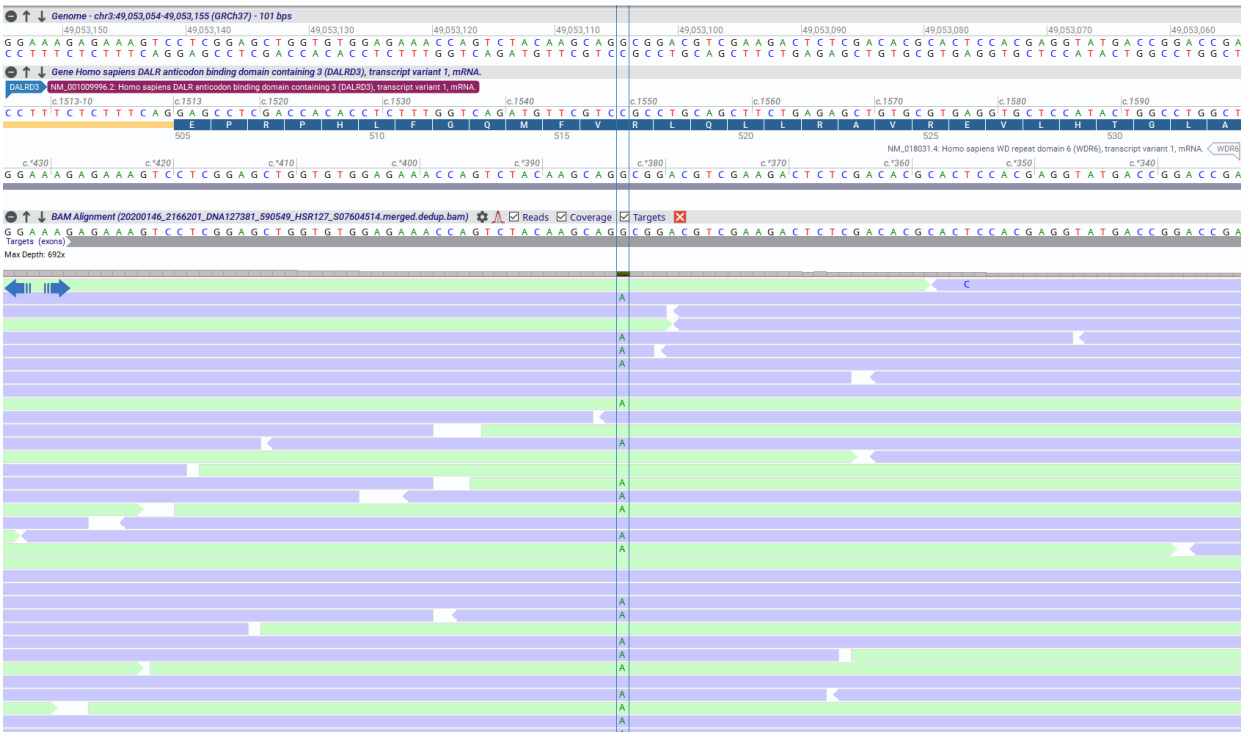

B Father

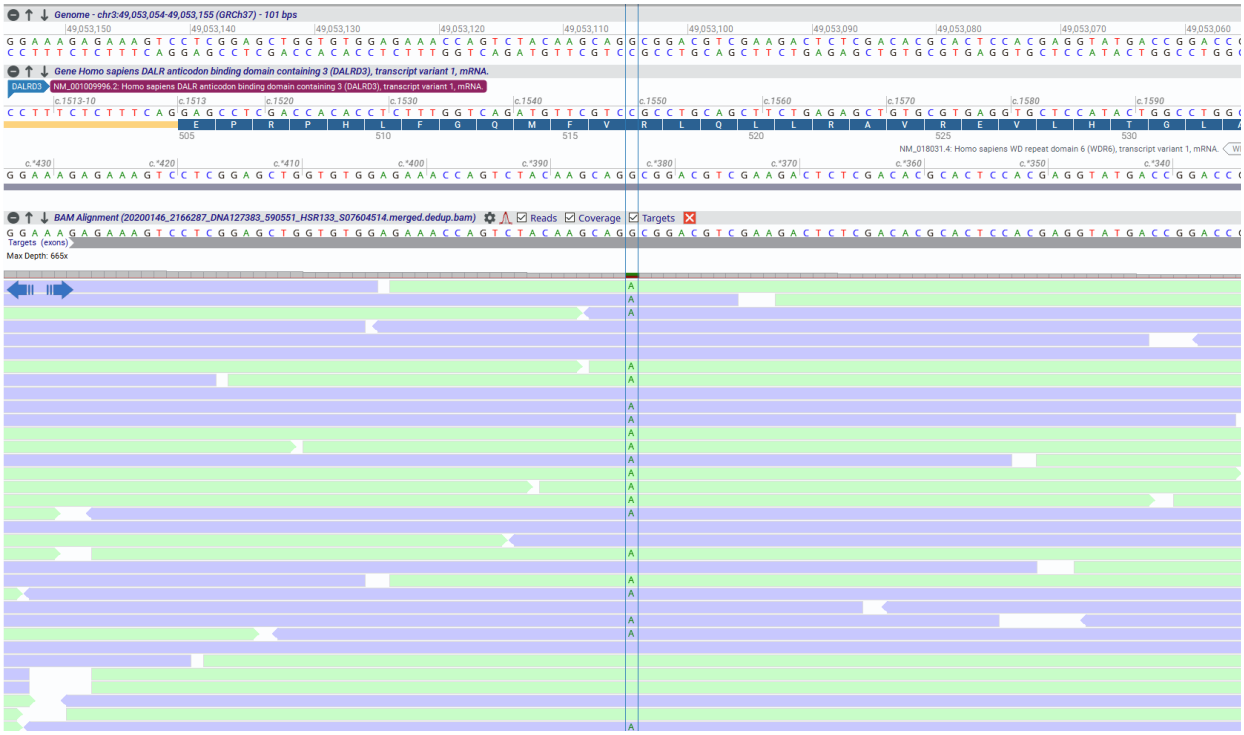

Supplemental Figure 5. The mother and father of the affected patient in this study are heterozygous carriers of the *DALRD3* missense variant. Whole exome sequence analysis of the (A) Mother and (B) Father.

Analysis	SIFT	PolyPhen	CADD	REVEL	MetaLR	Mutation taster
Score	0	1	31	0.906	0.871	82|40
Predicted outcome	Deleterious	Probably damaging	Likely deleterious	Likely disease causing	Damaging	Deleterious

Supplemental Figure 6. Scores and predicted outcomes for the R517C variant based upon the indicated pathogenicity prediction algorithms.

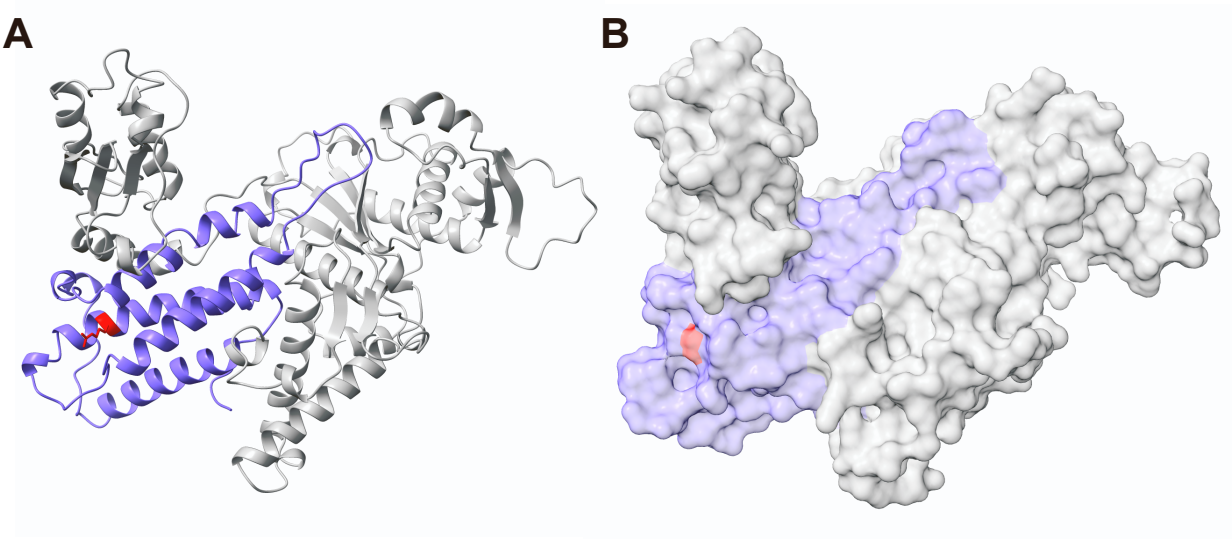

Supplemental Figure 7. (A) AlphaFold model of human DALRD3. The DALR anticodon binding domain is represented in violet and the R517 residue noted in red. (B) Surface plot of the predicted human DALRD3 structure with the R517 residue denoted in red.

Supplemental References

1. Corsten-Janssen, N., Bouman, K., Diphoorn, J.C.D., Scheper, A.J., Kinds, R., El Mecky, J., Breet, H., Verheij, J., Suijkerbuijk, R., Duin, L.K., et al. (2020). A prospective study on rapid exome sequencing as a diagnostic test for multiple congenital anomalies on fetal ultrasound. Prenat Diagn *40*, 1300-1309. 10.1002/pd.5781.

2. Ghorbani, F., Alimohamed, M.Z., Vilacha, J.F., Van Dijk, K.K., De Boer-Bergsma, J., Fokkens, M.R., Lemmink, H., Sijmons, R.H., Sikkema-Raddatz, B., Groves, M.R., et al. (2022). Feasibility of Follow-Up Studies and Reclassification in Spinocerebellar Ataxia Gene Variants of Unknown Significance. Front Genet *13*, 782685. 10.3389/fgene.2022.782685.

3. Ellard, S., Colclough, K., Patel, K.A., and Hattersley, A.T. (2020). Prediction algorithms: pitfalls in interpreting genetic variants of autosomal dominant monogenic diabetes. J Clin Invest *130*, 14-16. 10.1172/JCI133516.

4. Ramos, J., Proven, M., Halvardson, J., Hagelskamp, F., Kuchinskaya, E., Phelan, B., Bell, R., Kellner, S.M., Feuk, L., Thuresson, A.C., and Fu, D. (2020). Identification and rescue of a tRNA wobble inosine deficiency causing intellectual disability disorder. RNA *26*, 1654-1666. 10.1261/rna.076380.120.

5. Lentini, J.M., Alsaif, H.S., Faqeih, E., Alkuraya, F.S., and Fu, D. (2020). DALRD3 encodes a protein mutated in epileptic encephalopathy that targets arginine tRNAs for 3-methylcytosine modification. Nat Commun *11*, 2510. 10.1038/s41467-020-16321-6.